Desalination 432 (2018) 55–63

Contents lists available at ScienceDirect

Desalination

journal homepage: www.elsevier.com/locate/desal

Does electric or magnetic field affect reverse osmosis desalination?

Mohammad Razmkhah[a], Fatemeh Moosavi[b,*], Mohammad Taghi Hamed Mosavian[a], Ali Ahmadpour[a]

[a] Department of Chemical Engineering, Ferdowsi University of Mashhad, Mashhad 9177948944, Iran
[b] Department of Chemistry, Ferdowsi University of Mashhad, Mashhad 9177948974, Iran

GRAPHICAL ABSTRACT

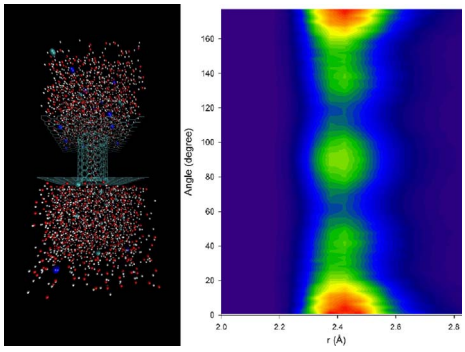

ARTICLE INFO

Keywords:
Magnetization
Electric field
Desalination
Molecular dynamics
Water flow rate

ABSTRACT

Effect of electric or magnetic field on desalination efficiency was studied by molecular dynamics simulation. A restricted double-walled carbon nanotube (CNT) was selected, then strong and weak external field regime were applied on simulated system. Results of simulation showed that strong electric field increases water flow rate two times than untreated system. Magnetization of water decreases water flow rate because of the increase in number of hydrogen bond. In addition, it was observed that applying electric field or magnetization of water completely rejects the ions. In fact, electric field moved back Na^+ ions because of the force acting on the ion opposite to the direction of reverse osmotic forces. Magnetization of water leads to a more stable hydration shell around the Na^+ ion that prevents passing through the carbon nanotube. In comparison with a single-walled CNT, considering a double-walled CNT enhances the experimental agreement of simulated water flow rate.

1. Introduction

Most of water supplies in the Earth are too salty for human consumption or are restricted to the polar ice. Food industry and agriculture are two main water industrial consumers that cannot utilize directly water from the salty seas water [1–2]. Therefore, water crisis is a problem that compromises the future of human life in the Earth. By growing the population, world societies warn about the shortage of water supplies. Desalination of salty water by reverse osmosis (RO) process introduces a way of increasing fresh water supplies.

However, desalination with RO process is still expensive for procurement of fresh water; therefore, economic and efficient desalination methods should be developed. Nanotube and nanopore have the potential to revolutionize desalination because they remove salt without any significant effect on the flow rate of water molecules [3–4].

In the field of computational study, many researches have an

* Corresponding author.
E-mail address: moosavibaigi@um.ac.ir (F. Moosavi).

https://doi.org/10.1016/j.desal.2017.12.062
Received 26 July 2017; Received in revised form 28 October 2017; Accepted 31 December 2017

attempt to investigate the effective parameters on the desalination process. Hummer et al. found that carbon nanotube (CNT) might conduct a chain of water molecules and protons [5], in good agreement with experiment [6–8]. Especially, the successful fabrication of aligned CNTs with membrane takes a solid step for practical application of CNTs in desalination [7,9–10]. Corry [11] conducted a comparison between differently sized carbon nanotubes. Corry reported that water conduction and ion rejection directly related to CNT diameter. He also reported that (6,6) CNT with diameter of 8.1 Å allows the water to pass and prevents passing the ions completely. However, flow rate of water was not appropriate for desalination process. Thus, Corry proposed a wider CNT which was selective to the water molecules by functionalizing the CNT entrance. This CNT increased water flow rate but could not completely prevent passing the ions [12]. Chan et al. [13] applied zwitterion functional groups to increase water flow rate. This functional group enhanced flow rate and rejected essentially all ions. To sum up, functionalization of CNT and controlling its entrance diameter are two important parameters playing role in the desalination.

Other parameters that do not have effect on desalination are also important because it help us to ignore them in the future study. Thomas et al. [14] reported that there is not a correlation between the CNT chirality and the internal fluid structure. Nicholls et al. [15] and Corry [11] showed that under the constant applied pressure, an increase in CNT length leads to a frictionless conductance inside the nanotube and negligible effect on the resulting water flow rate. Goldsmith et al. [16] demonstrated that the trend of water flow rate and ion rejection are independent of charge of carbon atoms in CNT.

There are many parameters including radius of CNT, functionalization of CNT, shape of CNT, etc. that could affect the rejection of ion and flow rate of water molecules. In current study, effect of external magnetic and electric field was investigated to find another parameter which affects desalination. Although many studies have been investigated the effect of external field on ion exchange membrane, it is not considered for desalination process.

Molecular dynamics (MD) simulations help us to study the mechanism of desalination at the molecular level which is still obscure. In addition, the thermodynamics and dynamics of desalination under external magnetic and electric field at molecular level are also very difficult to be studied experimentally. Accordingly, this study tries to understand the fundamental basis of external field effect on desalination process via a series of MD simulations.

Precisely, the main objective of this study is summarized as below:

- Investigating effect of applying external electric field on desalination (water flow rate and ion rejection)
- Studying the effect of magnetization on desalination efficiency
- Investigating for fast water conductor system
- Comparing the single-walled carbon nanotube (SWCNT) and double-walled carbon nanotube (DWCNT) for RO desalination

2. Methods

A DWCNT (with internal diameter of 8.1 Å and external diameter 10.2 Å and length of ~20 Å, see Fig. 1) was selected using force field parameters reported in ref. [17]. According to Corry [11–12] and Hummer et al. [5], all carbon charges were taken to be neutral because non-zero charges at the entrance of the CNT has a minor influence on water transfer and ion rejection properties of CNTs [18]. In other words, the major electrostatic barrier against passing the particle through a CNT mainly originates from the ion–water electrostatic interactions [19] (not water-carbon or ion-carbon electrostatic interaction).

This study applied the method introduced in ref. [20] to consider the reverse osmotic pressure. In fact, the CNT was confined between two inert walls as a support to model a more realistic CNT membrane, see ref. [20]. Supports are inert materials used to improve CNT mechanical stability [21–22].

The desalination process was simulated at high pressure of 25 MPa. In addition, a long time simulation (> 15 ns) was carried out at 2.4 MPa to compare the performance of CNTs for water desalination, see Section 3.5. It should be mentioned that external pressure applied in this study is approximately one order of magnitude greater than applicable values in the industry. Actually, in non-equilibrium MD simulations, it is common to reduce thermal noise and upgrade signal/noise ratio by this excessive pressure during a nanosecond timescale [23–24]. Besides, simulation cost significantly decreases at high pressure because of the faster water flow rate through CNT. At low pressure, the conductance of water occurs due to slow mechanism of molecular diffusion. In other words, simulation at low pressure is a time consuming process. Accordingly, it is reasonable to reduce simulation time by a high-pressure simulation.

A thick simple point charge (SPC) water layer [25] of ~30 Å width was placed on both sides of the membrane, Fig. 1b. At distances > 15 Å, a constant force was applied to water molecules from each side of the membrane (zone I in the Fig. 1b). Effect of using polarizable water was discussed in Supplementary data. The core shell model reported in ref. [26] was used to simulate polarizable flexible water. Results of polarizable water did not show a meaningful difference with SPC water.

To apply reverse osmotic pressure, a constant force acts on the molecules in control volume (zone I Fig. 1b). Because of this force, membrane (zone III Fig. 1b) may move along the force direction. To prevent translation of the membrane from its position, SHAKE algorithm [27] by tolerance of 1×10^{-5} was applied to the inert wall and all carbon atoms of CNT. The desalination process was simulated under constant temperature, 298 K, and volume (NVT ensemble) using Nose-Hoover thermostat [28]. Orthorhombic three-dimensional periodic boundaries measuring 65 Å in the z-direction and x–y plane of 29×29 Å^2 was considered for the simulation box (a detailed discussion about simulation box is given in section S.3 of Supplementary data). First, all systems were equilibrated for 1.5 ns under a constant pressure of 1 atm and temperature of 298 K; after that, 4.0 ns simulation with a time step of 2.0 fs was performed while the coordinates were saved every 0.1 ps for the further analysis.

In present study, the salty water contained 51 g/L Na^+ and Cl^- solvated in 1300 water molecules. A higher concentration salinity than seawater (~ 35 g/L) was selected to increase the ion-CNT interactions and attain more accurate results for a given system size and simulation time. The primitive intermolecular potential model was selected for modelling the ions [17]. In fact, primitive intermolecular potential model was derived by performing free energy perturbation simulations in aqueous solution. The minimum energies for the ions were also examined by this model and found to be in reasonable agreement with experiments [29]. Thus, this model was known as a reliable model for ion-water solutions.

The long-range electrostatic interactions were considered as Ewald summation method [30–31] with a 1×10^{-5} tolerance. The short-range van der Waals force was calculated within a cutoff distance of 11 Å (see section S.2, Supplementary data).

The electric force was applied by:

$$F = q.\ E,\ E(\mathrm{E_x}, \mathrm{E_y}, \mathrm{E_z}) \tag{1}$$

where, E is applied electric field vector (V·m^{-1}) and q is the atomic charge (C). In this study, we consider a strong and weak applied electric field as 10^6 and 10^3 V·m^{-1}, respectively. Elec1 and Elec2 abbreviations demonstrate the strong and weak electric field. In current study, electric field was applied opposite to the direction of reverse osmosis force.

The magnetic field was applied by:

$$F = q\ (v \times H),\quad H(\mathrm{H_x}, \mathrm{H_y}, \mathrm{H_z})\ \text{and}\ v(\mathrm{v_x}, \mathrm{v_y}, \mathrm{v_z}) \tag{2}$$

where H is the applied magnetic field vector (T) and v is the velocity vector (m·s^{-1}). In this study, we consider a strong and weak applied magnetic field as 10 and 1 T, respectively. Magn1 and Magn2

a)

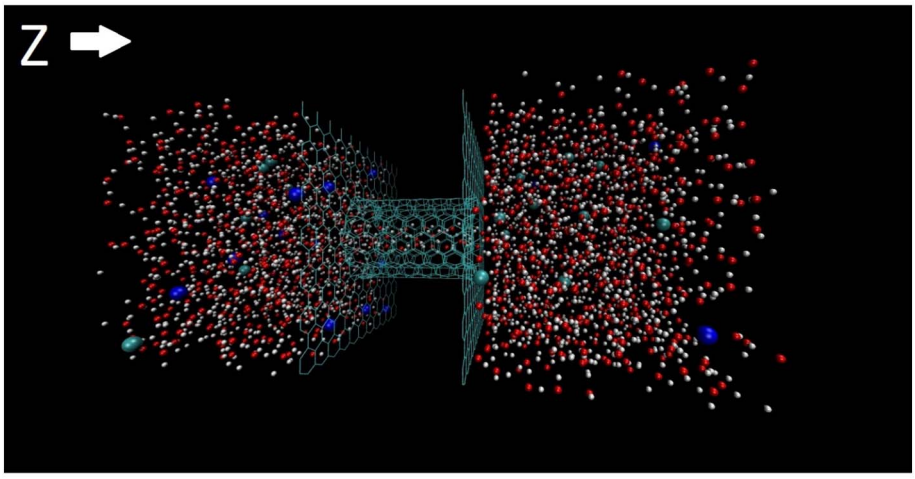

b)

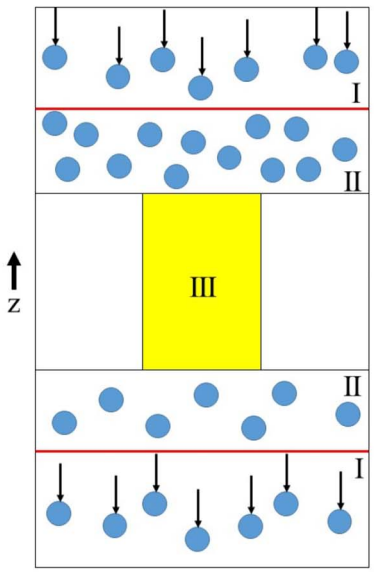

Fig. 1. a) Schematic of the CNT desalination system. Red, white, cyan, and dark blue colors represent the oxygen, hydrogen, Na^+, and Cl^-, respectively. b) Schematic of the CNT and applied reverse osmosis force; (I) represents the control volume of applied reverse osmosis force, (II) is the passing water zone, and (III) is the membrane zone. (For interpretation of the references to color in this figure legend, the reader is referred to the web version of this article.)

abbreviations demonstrate the strong and weak magnetic field. Magnetic field was applied opposite to the direction of reverse osmosis force.

Radial distribution function (RDF) was computed to analyze atomic correlation. RDF demonstrates the probability of finding a particle in a certain distance to another particle [18]:

$$g_{i,j}(r) = \frac{\rho(\mathrm{r})}{\rho} = \frac{V}{N_j}\frac{N_j(r)}{4\pi r^2 \Delta r} \tag{3}$$

where V is cell volume, N_j is total number of j atoms, and $N_j(\mathrm{r})$ is the number of j atoms in a spherical shell of Δr around i atoms.

Combination of angle and radial distribution functions were calculated to find the orientation of the water molecules. In this calculation, the phase space was separated into linear mesh then the RDF value collected into the linear RDF histogram and the angle distribution function (ADF) value into the linear ADF histogram. In other words, a two-dimensional mesh was applied into the RDF/ADF phase space. ADF is an angle distribution between a certain vector and a reference vector. We defined two different angles for ADF analysis as OW-HW…OW angle and hydration shell angle, Fig. 2a and b.

Potential of mean force (PMF) for the particles in the z-direction was calculated by means of the average densities in x-y plane using the fact that:

$$PMF(\mathrm{z}) = -kT\ln\left(\int \frac{\rho(\mathrm{z},\mathrm{r})}{\rho}\mathrm{dr}\right) = -kT\ln\left(\frac{\rho(\mathrm{z})}{\rho}\right) \tag{4}$$

where k is Boltzmann constant, T is temperature, and ρ is the number density. In addition, potential of mean force (PMF) for the particles as a function of r was calculated by:

$$PMF(r) = -kT\ln\left(\frac{\rho(\mathrm{r})}{\rho}\right) = -kT\ln g(\mathrm{r}) \tag{5}$$

The rolling average stack to 20,000 time steps was conducted between Δz or Δr slabs of 0.01 Å. First, the number of time-step used for the collection of the histograms is stated. Then each function is given in turn. The Simpson method was applied to calculate the integral.

DL_POLY_2.17 package [32–33] was developed to apply hydrostatic pressure in a specific region of simulation box, 15 Å on the either side of the membrane (zone I in Fig. 1b), and some in-house codes were developed for the further analyses.

3. Results and discussions

Table 1 shows the water flow rate of the studied systems. As can be seen from the table, applying a strong electrical field (Elec1) increases water conduction (approximately two times faster than No Field)

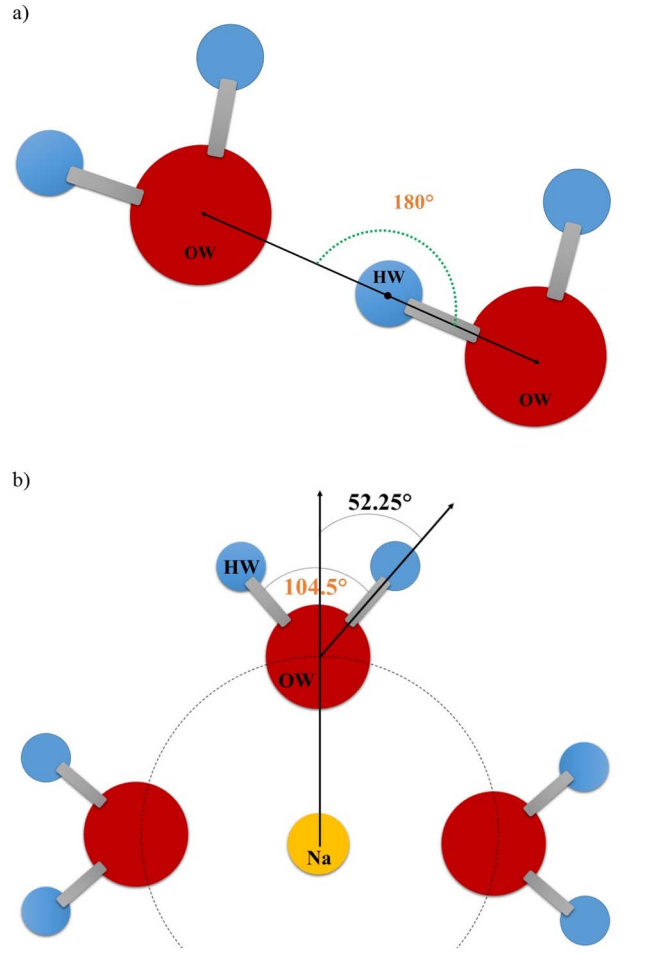

Fig. 2. Schematic of a) OW-HW…OW angle, b) a hydration shell and the ideal angle between Na-OW and OW-HW. OW and HW represent oxygen and hydrogen of water molecule, respectively.

Table 1
Water flow rate and percent of ion rejection under applied an external field.

System	Water flow rate (#/ns)	Ion rejection (%)
Elec1	11.75	100
Elec2	6.25	100
Magn1	2.75	100
Magn2	5.50	100
No field	5.25	96.87

shows number of water.

through the CNT. In spite that untreated system does not experience a complete ion rejection (96%), applying magnetic or electric field increases ion rejection to 100%. Even a weak electric field also increases water flow rate and ion rejection. However, strong magnetization deceases water conduction while increases ion rejection. In addition, weak magnetization leads to complete ion rejection and slightly increases water flow rate through the CNT. In the next sections, we discuss on water flow rate and ion rejection in more detail to find out what happens when an external field is applied in desalination process.

3.1. Water flow rate

In order to demonstrate that water force field does not play a significant role, the similar simulation was repeated by flexible polarizable water. The result showed that water flux does not observe any considerable change, see S.1 section of Supplementary data. It is known

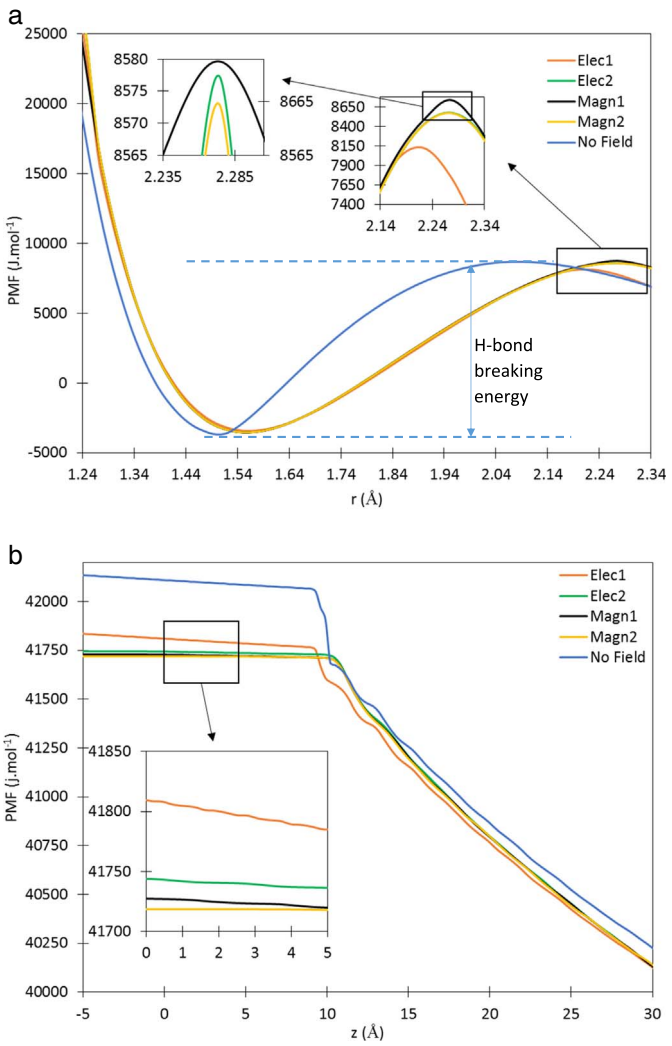

Fig. 3. a) PMF of OW-HW. The blue arrow shows the H-bond breaking energy for No Field system as a typical sample. The left corner small plot has two vertical axis. Right vertical axis is for Elec2 and Magn2 and left vertical axis scales the Magn1 PMF energy. b) PMF of water penetration. Note that the CNT starts from z = − 10 Å to z = 10 Å. Penetration energy is calculated by: $\Delta PMF = PMF_{tube} - PMF_{bulk}$. (For interpretation of the references to color in this figure legend, the reader is referred to the web version of this article.)

that water molecule is confined between a net of hydrogen bond (H-bond). This H-bond is broken at the entrance of the CNT to penetrate through the tube [20]. Accordingly, water flow possesses two steps: 1. H-bond breaking at the entrance of the tube and 2. water molecule penetration into the tube. In fact, step 1 depends on water-water interaction and step 2 depends on water-CNT interaction.

To investigate the H-bond breaking energy of the studied system, PMF(r) of OW-HW was calculated and reported in Fig. 3a. H-bond breaking energy is the amount of energy consumed for separating OW of a molecule from HW of another molecule. In this case, H-bond energy is the difference between the first minimum and maximum in the plot of PMF(r) of OW-HW, see blue arrow in Fig. 3a. As the figure shows, H-bond breaking energy substantially decreases by applying strong electric field; Table 2 reports amount of H-bond energy in detail. Besides, a weak electric field (Elec2) lowers the H-bond breaking energy; in contrast, strong water magnetization (Magn1) enhances H-bond energy. In other words, strong magnetization strengthens H-bond of water. Weak water magnetization decreases H-bond energy. We believe that the orientation of water molecule in the bulk is responsible for H-bond breaking energy, which will be discussed in Section 3.3.

Although H-bond PMF value of Elec2, Magn1, Magn2, and No Field

Table 2
PMF(r) of H-bond breaking and PMF(z) of water penetration. Number of H-bond averaged over simulation time.

System	PMF (r), H-bond energy (J·mol^{-1})	Number of H-bond per H_2O	PMF (z), Water penetration energy (J·mol^{-1})
Elec1	11,533.90	1.8745	1836.31
Elec2	12,082.11	1.9135	1744.32
Magn1	12,251.89	1.9534	1728.16
Magn2	12,090.87	1.9144	1718.46
No Field	12,183.48	1.9463	2283.76

are approximately close to each other, different water flow rates are observed in these cases. In fact, another parameter also affects water flow rate. It was found that number of H-bond intensifies effect of the H-bond PMF in water flow rate process. As Table 2 shows, number of H-bond in Elec1 is lower than other systems. This difference leads to faster water flow rate in Elec1. Number of H-bond obeys the same trend of water flow rate. Accordingly, amount of energy needed for H-bond breaking in addition to the lower number of H-bond in a high flow rate system are responsible for fast water flow rate through the tube.

After H-bond breaking, water penetrates through the tube. A water molecule should overcome the penetration barrier energy to cross through the tube. According to Table 2, penetration energy decreases by applying external field, see Fig. 3b. As the table shows, penetration energy decreases even by strong magnetization (Magn1). Easier penetration and lower H-bond breaking energy of Elec1 introduce it as a fast water conductor system.

3.2. Ion rejection

Based on Table 1, ion rejection of CNT is 96.87%. A complete ion rejection is achieved by applying external field to the system. Notice that ionic size of Na^+ is smaller than Cl^-. Because of this smaller size, Na^+ can penetrate through the tube. By rejecting Na^+, most of ions may be rejected resulting a complete ion rejection. Ions in the system are hydrated by water. This hydrated shell does not allow ions to penetrate into the tube because hydrated shell diameter (~7 Å) is larger than tube diameter (effective internal diameter assuming a carbon atom van der Waals radius of 4.7 Å) [11]. Accordingly, ion crosses through the tube due to two-step mechanism of dehydration and penetration. Dehydration energy is the amount of energy that is consumed for separating OW of a water molecule from Na^+. Similar to H-bond breaking energy, dehydration energy can be calculated from the difference between first minimum and maximum of PMF(r) of Na^+…OW (see Fig. 4a, black arrow). Table 3 also shows the dehydration energy in more detail. Fig. 4a demonstrates that the external field increases dehydration energy; the Elec1 system has the highest dehydration energy which increases the ion rejection of Na^+ in the system. Na^+ ions move opposite to the water flow rate because the electric field is opposite to the direction of water flow rate. Applying an electric field is more effective than magnetizing the system. Strong magnetization of water has lower dehydration barrier than weak one. Special orientation of hydrate shell can explain this observation (Section 3.3).

In addition to ion dehydration, penetration barrier energy is another parameter that affects ion rejection. By applying external field, penetration energy increases dramatically. This is the main reason of complete ion rejection when an external field is applied to the system. Similar to dehydration energy, applying electrical field has higher influence on penetration barrier than magnetization.

3.3. Special orientation of water molecules

Until now, we found out that the system with lower H-bond and penetration energy can easily conduct water. In contrast, higher dehydration and penetration energy is convenient for ion rejection

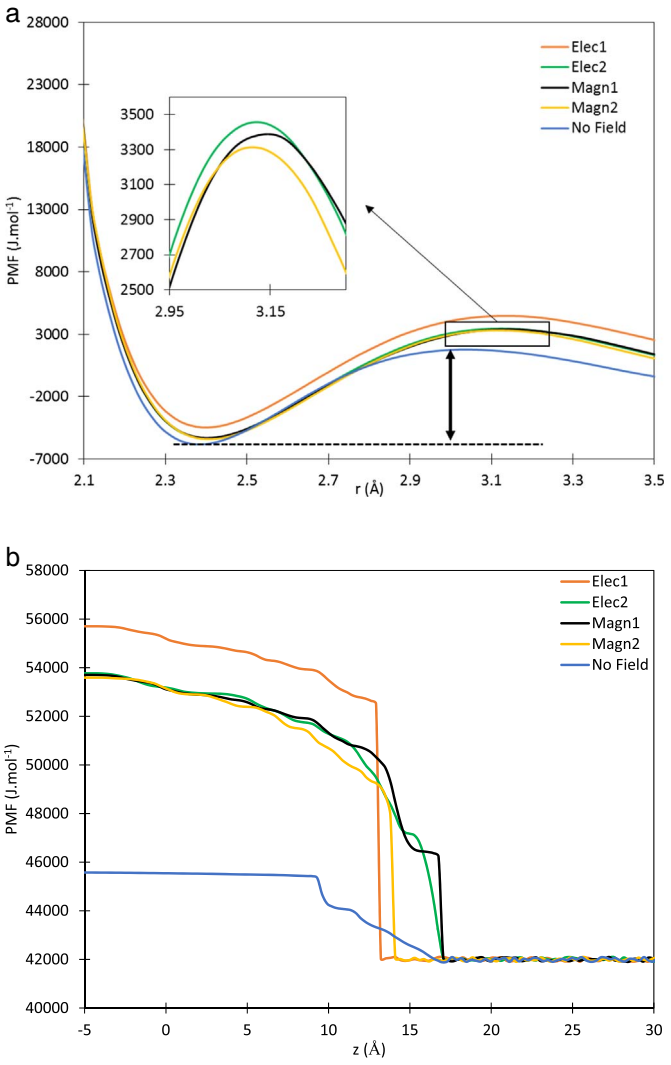

Fig. 4. PMF of a) ion dehydration. Black arrow shows the dehydration energy for No Field system as a typical sample. b) Penetration energy. Note that the CNT starts from z = −10 Å to z = 10 Å. Penetration energy is calculated by: $\Delta PMF = PMF_{tube} - PMF_{bulk}$.

Table 3
Na^+ dehydration and penetration PMF.

System	PMF (r), Ion dehydration (J·mol^{-1})	PMF(z), Ion penetration (J·mol^{-1})
Elec1	8882.56	12,590.04
Elec2	8760.16	10,642.96
Magn1	8651.08	10,511.52
Magn2	8699.97	10,383.89
No field	7597.29	3479.39

process. Here is an open question: how Elec1 conducts water faster and rejects ions more than other systems. The spatial orientation of H-bond nets and hydration sell of Na^+ was calculated to answer this question.

3.3.1. H-bond orientation

As mentioned before, hydrogen bonds should be broken at the tube entrance and then water molecule penetrates into the tube. It is best known that OW-HW…OW is a H-bond if the distance between HW and OW is < 2 Å and angle OW-HW…OW is about 180° [34]. Any deviation from these conditions leads to a weak H-bond. The H-bond angle (∠OW-HW…OW) distribution was calculated as a function of distance to investigate the effect of external field on the distribution, see Fig. 2a.

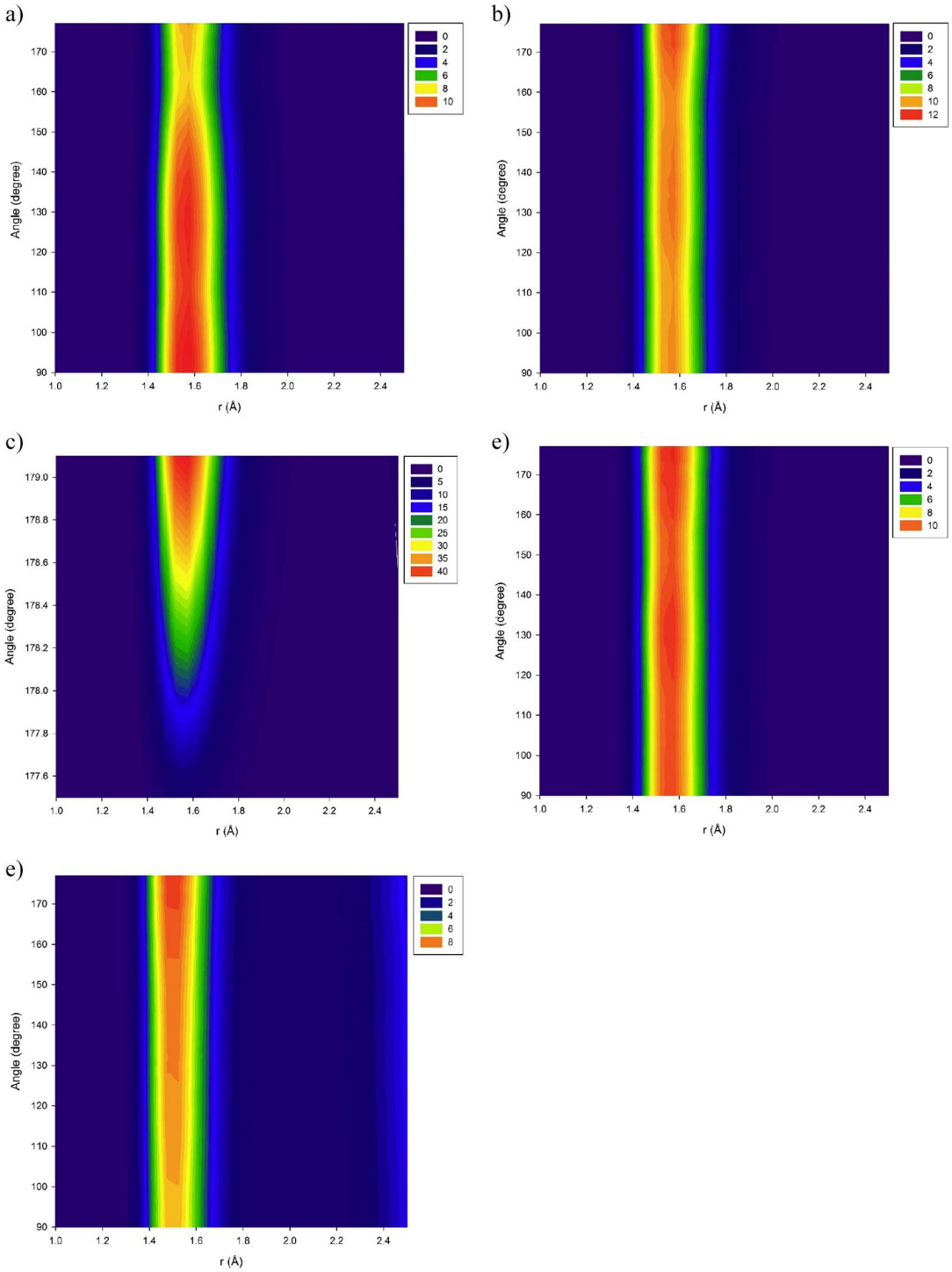

Fig. 5. ADF of H-bond angle as a function of distance for: a) Elec1, b) Elec2, c) Magn1, d) Magn2, and e) No Field.

Fig. 5 indicates that through the system HW…OW distance is < 2 Å while the angle distribution varies by changing the type of external field and its strength. As the figure shows, applying strong electric field leads to decrease probability of 180°, Fig. 5a. This is the main reason of the lowest barrier energy of H-bond in Elec1. In untreated system, the most probable angle is 180°, Fig. 5e. As can be seen from Fig. 5b, weak electrical field also propagates angle distribution into the central spectra. Strong magnetization of water compacts the angle distribution into 180°. This highly ordered structure of water in Magn1 is responsible for the highest H-bond energy. However, weak magnetization leads to a distribution of angle between 90° to 180°.

3.3.2. *Hydration shell orientation*

Actually, the number of water molecules is ideally 6 for the hydration shell of Na^+ ion and angle HW-OW-HW of a water molecule is 104.5°. Ideally, angle between OW-HW and Na-OW should be 52.25°, see Fig. 2b. Any deviation from this ideal angle leads to a degree of instability of hydration shell which weakens hydration shell interaction.

To investigate the orientation of water in hydration shell of Na^+, we calculated the angle distribution of Na^+…OW and OW-HW, see Fig. 6 for more detail. As Fig. 6a shows, angle distribution of 180° is more probable for hydration shell in Elec1. This orientation of hydration shell

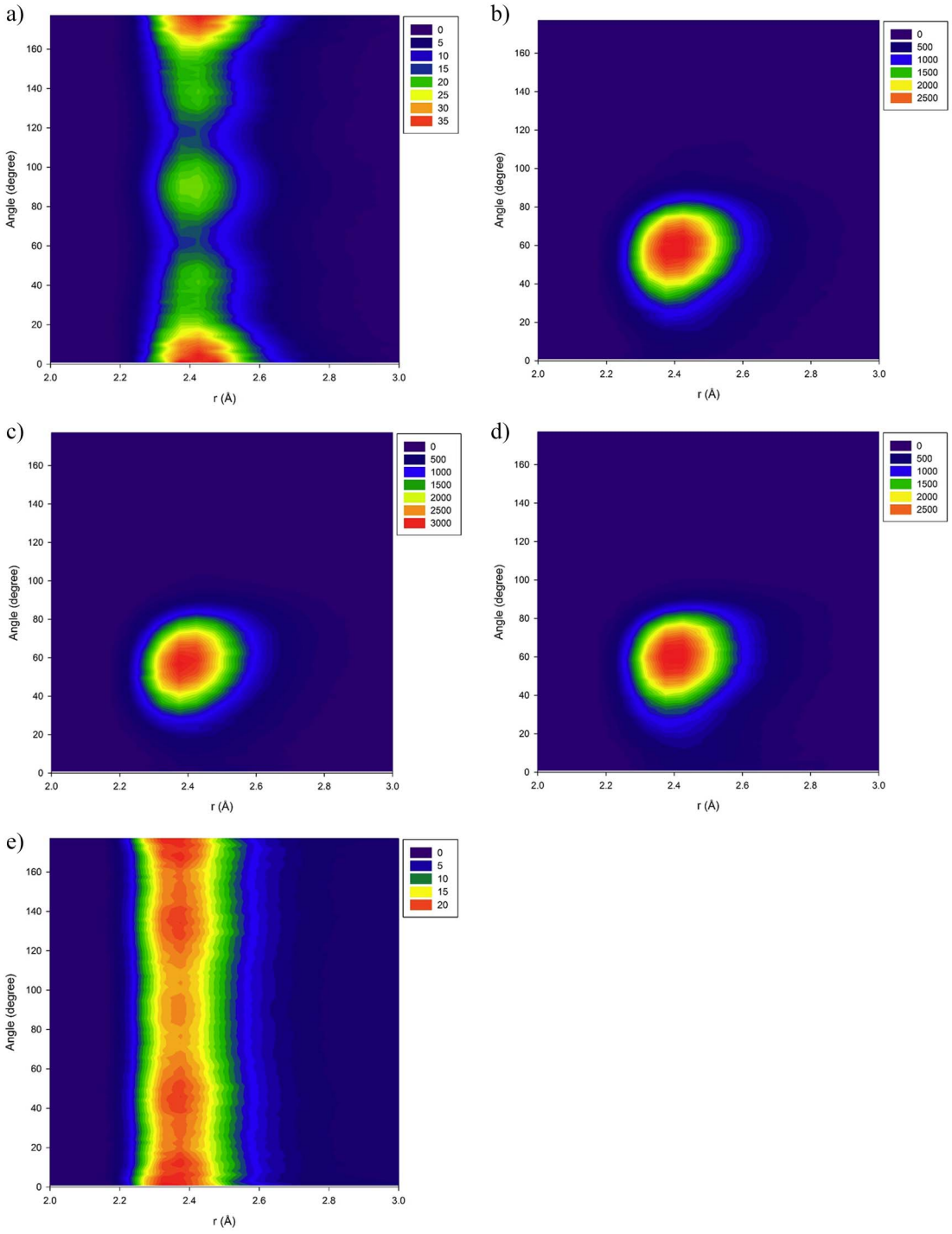

Fig. 6. ADF of hydration shell as function of distance for: a) Elec1, b) Elec2, c) Magn1, d) Magn2, and e) No Field.

Table 4
Number of water molecules in the hydration shell averaged over simulation time.

System	Na^+ hydration number
Elec1	3.68
Elec2	5.50
Magn1	5.30
Magn2	5.46
No Field	6.78

is not favorable. In fact, for the case of Elec1, all Na^+ ions are compacted to boundary of simulation box thus orientation angle of 180° becomes more probable. Strong electric field in Elec1 forces the Na^+ ions to move back (opposite to the direction of RO force). Consequently, this opposite force (electric force) is responsible for the complete ion rejection in the case of Elec1. Table 4 shows the average number of water molecules in the hydration shell of studied systems. Because of compacting Na^+ ion to the boundary of the system at Elec1, its hydration number is 3.68.

When a weak electric field is applied (Elec2), the hydration shell orients strongly around the ideal angle, Fig. 6b. This orientation is responsible for the higher energy of hydration, Table 3, and higher

hydration number, Table 4. In fact, the opposite force of weak electric field at Elec2 does not overcome the RO force; consequently, ions do not move backward.

Magnetization of water directly affects hydration shell orientation similar to Elec2, see Fig. 6c and d. Weak or strong magnetization forces the hydration shell to be ordered. This ordered structure leads to a stable hydration shell and consequently a complete ion rejection. Table 4 shows that the hydration number obeys the trend of hydration shell energy, Table 3. Totally, Elec2, Magn1, or Magn2 strengthens the hydration shell while strong opposite electric force is responsible for ion rejection in Elec1.

As can be seen from Fig. 6e, a distributed orientation occurs in hydration shell if the system is untreated. This orientation causes an unstable hydration shell around Na^+. Thus, conductance of ion becomes more probable. As Table 4 shows, the highest deviation from ideal number of hydration shell (6 water molecules) is in the case of untreated system, No Field. Note that ion rejection in Elec1 system is because of strong opposite electric force thus it is not comparable with other systems.

3.4. Comparing water conduction of double-walled and single-walled CNT

In the current study, we also compared desalination of a single-walled CNT with a double-walled CNT. A single-walled (6,6) CNT was simulated at 40 MPa with the method introduced in ref. [20] and 298 K to be compared with No Field system. H-bond energy is a function of operating condition (pressure and temperature), while penetration energy is a function of nature of membrane. Accordingly, we only compared the penetration energy because at constant pressure and temperature, H-bond energy for SWCNT and DWCNT systems are similar. Table 5 compares the PMF of water conduction in SWCNT and DWCNT.

As Table 5 shows, water penetration in SWCNT is more favorable than DWCNT system. Reason of such behavior can be arisen from the additional interaction between two walls of DWCNT and water molecules. Result of easier water penetration is reflected on the water flow rate, see next section. We believe that an extra number of wall, more than two walls, does not affect obviously on water penetration because the distance of third and fourth walls of CNT are rationally far from the center of water conduction channel. Further analysis on this subject would be valuable, in the future.

3.5. Performance of desalination

It would be valuable to investigate applicability and validity of the simulated CNT system by comparing with experimental results. Accordingly, we conduct the long time simulations (> 15 ns) at low pressure (2.4 MPa) to compare and validate our results with the real systems, see Table 6. All of the simulated CNTs showed a complete salt rejection. According to previous study [20], at a pressure lower than 50 MPa, a complete salt rejection can be expected for (6,6) CNT.

As can be seen from Table 6, water flow rate in the No Field (DWCNT) system is rationally in good agreement with experiment [6–8]. Accordingly, considering a double-walled CNT is more accurate than a single-walled CNT [20]. Experimental results were extrapolated to the simulation pressure drop. This study simulated water flow rate driven by an osmotic pressure of 2.4 atm. However, the experiments reported pressure drops of 0.1 MPa [6–7], and 0.069 MPa [8]. Based on Corry's results [11], there is no problem to extrapolate experimental results to 2.4 MPa because the water flow rate is a linear function of the applied pressure. Therefore, a linear extrapolation can be used as an approximation to compare our calculated flow rate with experimental results. We observe two key differences between the simulation and experiment: 1. CNT diameter used in experiment was 16 Å on average, while our simulation used nanotubes with a diameter of 8.1 Å; 2. the pressure drops were 0.1 MPa, and 0.069 MPa in the experiments versus 2.4 MPa in our simulations.

Results of water flow rate in the current study are in appropriate agreement with the experiment. Thus, these results are reliable for using in a real experiment. As the table demonstrates, Elec1 conducts water approximately two times faster than No Field system. Thus, applying strong electrical field can be used to increase the efficiency of desalination process.

Overall, our results indicate that CNT may act as a high-efficient desalination membrane. Among the desalination applied external field that exhibited both water conduction and full salt rejection, the water permeability at 2.4 MPa ranged from 4.01 to 8.32 L per cm^2·day, Fig. 7. These simulations propose that very large flow rate can be expected in all the studied systems, especially Elec1. Indeed, Elec1 could be expected to 100% desalination with a flow rate of over 10 times that of existing membranes.

Table 5
Penetration PMF of SWCNT and DWCNT at the absence of electric or magnetic field (No Field).

System	Penetration energy ($J \cdot mol^{-1}$)
DWCNT (no field)	2283.76
SWCNT	2004.84

Table 6
Comparison between simulation and different experiments.

Membrane	Diameter (Å)	Conductance ($L \cdot cm^{-2} \cdot day^{-1}$)	Pore density ($pore \cdot cm^{-2}$)	Ref.
Elec1	8.1	8.32	2.4×10^{11}	This study
Elec2	8.1	4.93	2.4×10^{11}	This study
Magn1	8.1	1.23	2.4×10^{11}	This study
Magn2	8.1	4.50	2.4×10^{11}	This study
DWCNT (No Field)	8.1	4.01	2.4×10^{11}	This study
(6,6) SWCNT	8.1	4.75	2.4×10^{11}	[20]
(6,6) SWCNT	8.1	0.27	2.4×10^{11}	[11]
CNT	< 20	3.09	–	[8]
CNT	< 20	15.35	2.4×10^{11}	[7]
CNT	< 65	69.12	0.81×10^{11}	[6]

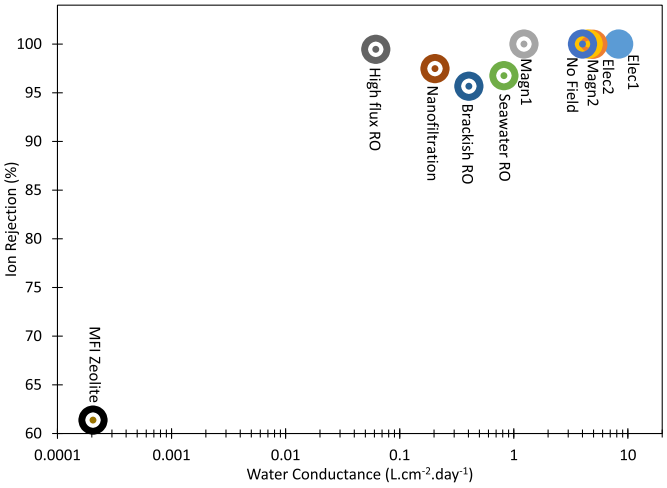

Fig. 7. Performance chart for different studied CNTs versus existing industrial technologies. Studied CNTs in this work could desalinate salt completely with a flow rate of over 100 times that of commercial technology. The data for RO and MFI zeolites is adapted from Pendergast et al. [35].

4. Conclusion

It was observed that applying strong electric field effectively increases the water flow rate and ion rejection. There are three parameters important for water conduction: H-bond PMF, number of H-bond, and penetration PMF. H-bond PMF of water in Elec1 system was obviously the lowest. In addition, penetration barrier energy decreases by applying any external field to the system. Note that orientation of H-bond angle is responsible for H-bond PMF. The faster flow rate one system has, the higher deviation from ideal angle (180°) it experiences. Strong magnetization of water increases the H-bond PMF and decreases water flow rate.

By applying any external field, complete ion rejection was observed for each system. Applying electric field causes to a backward force (opposite to the reverse osmosis force) to Na^+ ion. This opposite force increases the barrier against Na^+ ion to pass through the CNT. Magnetization of water increases the stability of hydration shell.

To sum up, desalination of water effectively is increased by applying electric field. However, magnetization of water is not an effective way to increase desalination efficiency.

Acknowledgment

The financial support provided by Ferdowsi University of Mashhad of Iran (Grant No. 3/43730) is greatly appreciated.

Appendix A. Supplementary data

Supplementary data to this article can be found online at https://doi.org/10.1016/j.desal.2017.12.062.

References

[1] W. Cao, C. Beggs, I.M. Mujtaba, Theoretical approach of freeze seawater desalination on flake ice maker utilizing LNG cold energy, Desalination 355 (2015) 22–32.
[2] Y. Wang, Z. He, K.M. Gupta, Q. Shi, R. Lu, Molecular dynamics study on water desalination through functionalized nanoporous graphene, Carbon 116 (2017) 120–127.
[3] M. Thomas, B. Corry, T.A. Hilder, What have we learnt about the mechanisms of rapid water transport, ion rejection and selectivity in nanopores from molecular simulation? Small 10 (8) (2014) 1453–1465.
[4] A. Ozcan, C. Perego, M. Salvalaglio, M. Parrinello, O. Yazaydin, Concentration gradient driven molecular dynamics: a new method for simulations of membrane permeation and separation, Chem. Sci. 8 (2017) 3858–3865.
[5] G. Hummer, J.C. Rasaiah, J.P. Noworyta, Water conduction through the hydrophobic channel of a carbon nanotube, Nature 414 (6860) (2001) 188–190.
[6] B. Lee, Y. Baek, M. Lee, D.H. Jeong, H.H. Lee, J. Yoon, Y.H. Kim, A carbon nanotube wall membrane for water treatment, Nat. Commun. 6 (2015) 7109.
[7] J.K. Holt, H.G. Park, Y. Wang, M. Stadermann, A.B. Artyukhin, C.P. Grigoropoulos, A. Noy, O. Bakajin, Fast mass transport through sub-2-nanometer carbon nanotubes, Science 312 (5776) (2006) 1034–1037.
[8] F. Fornasiero, H.G. Park, J.K. Holt, M. Stadermann, C.P. Grigoropoulos, A. Noy, O. Bakajin, Ion exclusion by sub-2-nm carbon nanotube pores, Proc. Natl. Acad. Sci. 105 (45) (2008) 17250–17255.
[9] S. Kim, F. Fornasiero, H.G. Park, J.B. In, E. Meshot, G. Giraldo, M. Stadermann, M. Fireman, J. Shan, C.P. Grigoropoulos, Fabrication of flexible, aligned carbon nanotube/polymer composite membranes by in-situ polymerization, J. Membr. Sci. 460 (2014) 91–98.
[10] S. Kim, J.R. Jinschek, H. Chen, D.S. Sholl, E. Marand, Scalable fabrication of carbon nanotube/polymer nanocomposite membranes for high flux gas transport, Nano Lett. 7 (9) (2007) 2806–2811.
[11] B. Corry, Designing carbon nanotube membranes for efficient water desalination, J. Phys. Chem. B 112 (5) (2008) 1427–1434.
[12] B. Corry, Water and ion transport through functionalised carbon nanotubes: implications for desalination technology, Energy Environ. Sci. 4 (3) (2011) 751–759.
[13] W.-F. Chan, H.-Y. Chen, A. Surapathi, M.G. Taylor, X. Shao, E. Marand, J.K. Johnson, Zwitterion functionalized carbon nanotube/polyamide nanocomposite membranes for water desalination, ACS Nano 7 (6) (2013) 5308–5319.
[14] B. Huang, A. McGaughey, M. Kaviany, Thermal conductivity of metal-organic framework 5 (MOF-5): part I. Molecular dynamics simulations, Int. J. Heat Mass Transf. 50 (3) (2007) 393–404.
[15] W.D. Nicholls, M.K. Borg, J.M. Reese, Molecular dynamics simulations of liquid flow in and around carbon nanotubes, ASME 2010 8th International Conference on Nanochannels, Microchannels, and Minichannels Collocated With 3rd Joint US-European Fluids Engineering Summer Meeting, American Society of Mechanical Engineers, 2010, pp. 979–985.
[16] J. Goldsmith, C.C. Martens, Molecular dynamics simulation of salt rejection in model surface-modified nanopores, J. Phys. Chem. Lett. 1 (2) (2009) 528–535.
[17] A.T. Nasrabadi, M. Foroutan, Ion-separation and water-purification using single-walled carbon nanotube electrodes, Desalination 277 (1) (2011) 236–243.
[18] M. Thomas, B. Corry, A computational assessment of the permeability and salt rejection of carbon nanotube membranes and their application to water desalination, Phil. Trans. R. Soc. A 374 (2060) (2016) 20150020.
[19] J.H. Park, S.B. Sinnott, N. Aluru, Ion separation using a Y-junction carbon nanotube, Nanotechnology 17 (3) (2006) 895.
[20] M. Razmkhah, A. Ahmadpour, M.T.H. Mosavian, F. Moosavi, What is the effect of carbon nanotube shape on desalination process? A simulation approach, Desalination 407 (2017) 103–115.
[21] J. Prince, S. Bhuvana, V. Anbharasi, N. Ayyanar, K. Boodhoo, G. Singh, Ultra-wetting graphene-based membrane, J. Membr. Sci. 500 (2016) 76–85.
[22] P.S. Goh, A.F. Ismail, Review: is interplay between nanomaterial and membrane technology the way forward for desalination? J. Chem. Technol. Biotechnol. 90 (6) (2015) 971–980.
[23] Q. Chen, X. Yang, Pyridinic nitrogen doped nanoporous graphene as desalination membrane: molecular simulation study, J. Membr. Sci. 496 (2015) 108–117.
[24] Z. Hu, J. Jiang, Separation of amino acids in glucose isomerase crystal: insight from molecular dynamics simulations, J. Chromatogr. A 1216 (26) (2009) 5122–5129.
[25] Y. Wu, H.L. Tepper, G.A. Voth, Flexible simple point-charge water model with improved liquid-state properties, J. Chem. Phys. 124 (2) (2006) 024503.
[26] K. Ganesh, A.D. Sanket, K.R.S.S. Subramanian, Comparison of select polarizable and non-polarizable water models in predicting solvation dynamics of water confined between MgO slabs, J. Phys. Condens. Matter 25 (30) (2013) 305003.
[27] J.-P. Ryckaert, G. Ciccotti, H.J. Berendsen, Numerical integration of the Cartesian equations of motion of a system with constraints: molecular dynamics of n-alkanes, J. Comput. Phys. 23 (3) (1977) 327–341.
[28] D.J. Evans, B.L. Holian, The nose–hoover thermostat, J. Chem. Phys. 83 (8) (1985) 4069–4074.
[29] J. Aqvist, Ion-water interaction potentials derived from free energy perturbation simulations, J. Phys. Chem. 94 (21) (1990) 8021–8024.
[30] A.Y. Toukmaji, J.A. Board, Ewald summation techniques in perspective: a survey, Comput. Phys. Commun. 95 (2–3) (1996) 73–92.
[31] P.P. Ewald, Die Berechnung optischer und elektrostatischer Gitterpotentiale, Ann. Phys. 369 (3) (1921) 253–287.
[32] W. Smith, T.R. Forester, DL_POLY_2.0: a general-purpose parallel molecular dynamics simulation package, J. Mol. Graph. 14 (3) (1996) 136–141.
[33] W. Smith, Guest editorial: DL_POLY–applications to molecular simulation II, Mol. Simul. 32 (12 – 13) (2006) (933–933).
[34] F. Moosavi, F. Abdollahi, M. Razmkhah, Int. J. Greenhouse Gas Control 37 (2015) 158–169.
[35] M.M. Pendergast, E.M. Hoek, A review of water treatment membrane nanotechnologies, Energy Environ. Sci. 4 (6) (2011) 1946–1971.